energies

MDPI

Article

Optimization of Expressway Microgrid Construction Mode and Capacity Configuration Considering Carbon Trading

Lei Yao [1,2], Chongtao Bai [3], Hao Fu [2], Suhua Lou [3,*] and Yan Fu [3]

[1] School of Economics, Wuhan University of Technology, Wuhan 430072, China; lyy@cggc.cn
[2] Gezhouba Group Transportation Investment Co., Ltd., Wuhan 430030, China; fuhao20951@cggc.cn
[3] State Key Laboratory of Advanced Electromagnetic Engineering and Technology, Huazhong University of Science and Technology, Wuhan 430074, China; chongtao_bai@hust.edu.cn (C.B.); m202372470@hust.edu.cn (Y.F.)
* Correspondence: shlou@mail.hust.edu.cn

Abstract: An expressway microgrid can make full use of renewable resources near the road area and enable joint carbon reduction in both transportation and energy sectors. It is important to research the optimal construction mode and capacity configuration method of expressway microgrid considering the carbon trading and carbon offset mechanism. This paper establishes a design model for an expressway microgrid considering the operating features of each component in the microgrid under two patterns of grid-connected/islanded and two types of AC/DC. The goal of the proposed model is to minimize the annualized comprehensive cost, which includes the annualized investment cost, operational cost, and carbon trading cost. The model designates the optimal construction mode of an expressway microgrid, i.e., grid-connected or islanded, AC or DC. As a mixed integer nonlinear programming (MINLP) problem, the proposed model can be solved in a commercial solver conveniently, such as GUROBI and CPLEX. The validity and practicality of the proposed model have been demonstrated through case studies in several different application scenarios, which also demonstrate the necessity of considering carbon trading mechanisms in the design model.

Keywords: microgrid planning; expressway microgrid construction mode; AC/DC microgrid; carbon trading mechanism

Citation: Yao, L.; Bai, C.; Fu, H.; Lou, S.; Fu, Y. Optimization of Expressway Microgrid Construction Mode and Capacity Configuration Considering Carbon Trading. *Energies* **2023**, *16*, 6720. https://doi.org/10.3390/en16186720

Academic Editor: Abu-Siada Ahmed

Received: 25 July 2023
Revised: 14 September 2023
Accepted: 18 September 2023
Published: 20 September 2023

1. Introduction

With the depletion of fossil energy and increasingly serious environmental problems, carbon reduction from both the energy and transport sectors is an important way to help achieve carbon neutrality [1,2]. Electric vehicles (EV) and solar energy-powered expressways are considered a promising approach for sustainable development in both the energy and transport sectors [3–5]. In recent years, the rapid growth of EV ownership has led to an increasing demand for charging on expressways. On one hand, expressway service areas are usually located in remote areas, and the existing distribution network is incapable of carrying several charging points for EVs charging simultaneously [6,7]. On the other hand, when DC charging points are integrated with DC components, such as photovoltaic power generation and battery energy storage into the DC system, it can reduce power loss during the AC–DC conversion process and achieve greater economic benefits [8]. The traditional AC grid-connected construction mode of expressway service areas may no longer be applicable. Besides EV charging loads, expressways also include various AC loads, such as tunnel ventilation and lighting, service area cooling and heating, monitoring and communication, etc.; therefore, it is of great practical significance to determine the best expressway microgrids construction mode (AC/DC, grid-connected/islanded) and optimize the capacity configuration while considering the limitations of the installed capacity of renewable energy generation and AC/DC loads structure in different load centers. In addition, with the constant development and improvement of the global carbon

market, expressway microgrids with a large amount of renewable energy generation have the opportunity to obtain significant revenue from the carbon market [9], which can promote energy transition and affect the construction mode of expressway microgrids. It is also an important factor in promoting the green economy on the expressway system.

At present, the problems of expressway microgrid planning are mainly focused on the location of charging stations and capacity optimization of generators and battery energy storage. Reference [10] proposed a mathematical model of EV charging demand at a rapid charging station for the planning of an expressway distribution system based on the fluid dynamic traffic model and the M/M/s queueing theory. To consider the waiting time of EV users and the operating cost of station operators, references [11,12] proposed a charging station multi-objective planning model based on dynamic traffic flow simulation on expressways. In terms of the AC/DC microgrid planning, reference [13] developed a combinatorial optimization technology to solve the optimal selection problem of AC/DC hybrid microgrid and pointed out that using different types of energy storage and properly distinguishing loads is conducive to reducing the total cost of the microgrid. References [14,15] proposed a microgrid planning model to determine the optimal size and generation combination of distributed power sources in microgrids, as well as the type of microgrid. With the increasing proportion of distributed power sources and DC loads, DC microgrids may be more advantageous than AC microgrids [14–16]. For an interconnected microgrid, reference [17] introduced the concept of a DC power exchange expressway to interconnect AC microgrid clusters on the expressway. In order to increase the flexibility of a banded featured microgrid, reference [18] proposed a new evolutionary model of a railway energy supply system for railway PV integration systems by constructing a three-in-one traction–storage–information integrated station. Reference [19] compared the technical and economic benefits of several configurations of solar energy integration into the railway microgrid and proposed a design methodology for selecting the railway power supply components. In terms of the carbon trading mechanism in a microgrid, references [20,21] established low-carbon economic operation models of microgrid systems considering carbon capture technology, which can significantly reduce the carbon emissions of microgrids. Reference [22] proposed a joint IGDT dispatch strategy for a microgrid cluster considering the tiered carbon price and quantified the uncertainty of wind and PV factors on dispatching operations.

Currently, a carbon trading mechanism is most often applied in the optimal scheduling of microgrid systems, and there is little research on the decision method or design model for the construction mode selection of an expressway microgrid considering a carbon trading mechanism.

The main contributions of this paper are summarized as follows:

(1) This paper proposes a MINLP model that includes carbon trading and a carbon offset mechanism for optimizing the construction mode and capacity configuration of expressway microgrids with various energy sources. In addition, this paper compares the effects of different source-load structures on the optimal construction mode selection.
(2) The necessity and validity of taking carbon trading mechanism into account is investigated by comparing the planning results with different carbon trading models.
(3) The effects of the changing of CER trading price on the optimal construction mode selection are compared.

The rest of this paper is organized as follows. Section 2 provides a brief overview of the problem. Section 3 uses a probabilistic approach to model renewable energy generation output. Section 4 establishes a design model that considers the carbon trading and carbon offset mechanism to decide the optimal construction mode and capacity configuration of an expressway microgrid. Section 5 presents the case study, and Section 6 offers conclusions.

2. Problem Statement

The structure of an expressway microgrid is shown in Figure 1, which is divided into two types of AC/DC and two patterns of a grid-connected/islanded microgrid for a total of four construction modes. In order to facilitate the description, the DC grid-connected mode, AC grid-connected mode, DC islanded mode, and AC islanded mode are referred to as mode 1 to 4, respectively. The islanded pattern includes wind power, photovoltaic power generation, diesel generator, battery energy storage, and AC and DC loads. The grid-connected pattern includes transmission lines and transformers between the microgrid and distribution network but does not require the configuration of diesel generators. Since both power sources and loads are divided into AC and DC, the corresponding converters need to be configured according to the microgrid type. Note that the static var compensator (SVC) needs to be configured for reactive power balancing to address voltage stabilization in the AC microgrid.

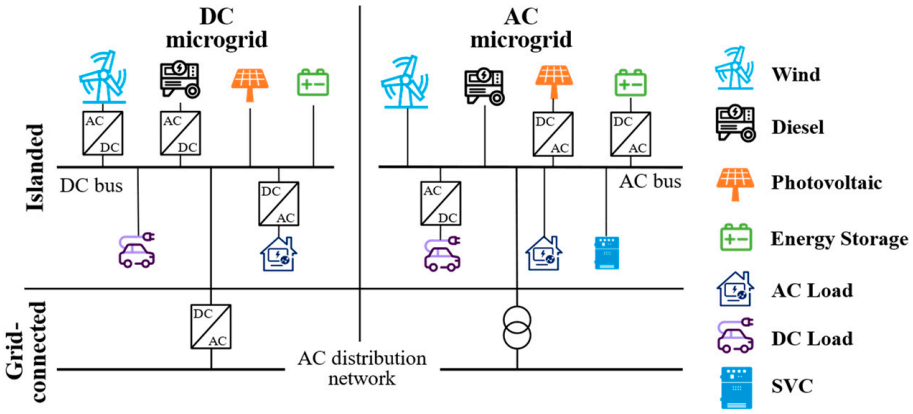

Figure 1. Schematic diagram of the expressway microgrid structure.

With the carbon offset mechanism and certified emission reduction (CER) trading, which is indicated in Section 4.1, a large amount of renewable energy generation can obtain significant profits from the carbon trading market; therefore, this paper takes the carbon trading and carbon offset mechanism into account and proposes a design model that aims at minimizing the annualized investment cost, operational cost, and carbon trading cost of the expressway microgrid.

3. Probabilistic Renewable Energy Generation Modeling

3.1. Modeling of Solar Irradiance and PV Module Output Power

In order to take into account the random possibility of cloud cover, the solar irradiance is modeled by the probability density function (PDF) of clearness index K_T, which is defined as the ratio of the horizontal irradiance to the extraterrestrial total solar irradiance. The PDF of clearness index can be expressed as Equation (1).

$$P(K_T) = \alpha_{\mathrm{CI}} \frac{(K_{TU} - K_T)}{K_{TU}} e^{\lambda_{\mathrm{CI}} K_T} \tag{1}$$

In Equation (1), K_{TU} is the maximum value of the clearness index. α_{CI} and λ_{CI} are functions of the maximum value and mean value K_{TM} of the clearness index as follows [23]:

$$\alpha_{\mathrm{CI}} = \frac{{\lambda_{\mathrm{CI}}}^2 K_{TU}}{e^{\lambda_{\mathrm{CI}} K_{TU}} - \lambda_{\mathrm{CI}} K_{TU} - 1} \tag{2}$$

$$\lambda_{\mathrm{CI}} = \frac{2\gamma_{\mathrm{CI}} - 17.519 e^{-1.3118\gamma_{\mathrm{CI}}} - 1062 e^{-5.0426\gamma_{\mathrm{CI}}}}{K_{TU}} \tag{3}$$

$$\gamma_{\mathrm{CI}} = \frac{K_{TU}}{K_{TU} - K_{TM}} \tag{4}$$

Based on the definition of the clearness index, the solar irradiance I_β on a PV panel with inclination β can be calculated as in Equation (5).

$$I_\beta = \left[\left(R_b + \rho\frac{1-\cos\beta}{2}\right) + \left(\frac{1+\cos\beta}{2} - R_b\right)p_{kd}\right] I_O K_T - \left(\frac{1+\cos\beta}{2} - R_b\right) q_{kd} I_O {K_T}^2 \tag{5}$$

In Equation (5), R_b is the ratio of beam radiation on a tilted surface to a horizontal surface. ρ is the reflectance of the ground. p_{kd} and q_{kd} are the linearized parameters for diffuse radiation on a horizontal plane. I_O is the extraterrestrial total solar irradiance.

With the hourly clearness index PDF in different seasons and utilizing the Monte Carlo simulation technique, the hourly solar irradiance in different seasons can be calculated in Equation (5). The PV module output power in different seasons can be calculated as follows [24]:

$$P_{\mathrm{PV}} = P_{\mathrm{S}}\frac{I_\beta}{I_{\mathrm{S}}}\left[1 + k_{\mathrm{p}}(T_c - T_{\mathrm{S}})\right] \tag{6}$$

In Equation (6), P_{PV} is the PV available output power. P_{S}, I_{S}, and T_{S} are the rated output power, solar irradiance, and PV module temperature under standard test conditions, respectively. k_{p} is the power temperature coefficient. T_c is the PV module temperature of the operating environment.

3.2. Modeling of Wind Speed and Wind Turbine Output Power

In this paper, the wind speed is modeled by the Weibull distribution, as in Equation (7):

$$f(v_{\mathrm{w}}) = \frac{k}{c}\left(\frac{v_{\mathrm{w}}}{c}\right)^{k-1} e^{-(v_{\mathrm{w}}/c)^k} \tag{7}$$

In Equation (7), $f(v_{\mathrm{w}})$ is the distribution probability of wind speed v_{w}. K and c are the shape and scale parameter, respectively, which can be calculated by many different methods [23].

With the hourly wind speed PDF in different seasons and the Monte Carlo simulation technique, the hourly wind turbine output power in different seasons can be calculated as follows:

$$P_{\mathrm{w}} = \begin{cases} 0, & v_{\mathrm{w}} \le v_{\mathrm{ci}} \text{ or } v_{\mathrm{w}} \ge v_{\mathrm{co}} \\ P_{\mathrm{rated}}\frac{v_{\mathrm{w}} - v_{\mathrm{ci}}}{v_{\mathrm{r}} - v_{\mathrm{ci}}}, & v_{\mathrm{ci}} \le v_{\mathrm{w}} \le v_{\mathrm{r}} \\ P_{\mathrm{rated}}, & v_{\mathrm{r}} \le v_{\mathrm{w}} \le v_{\mathrm{co}} \end{cases} \tag{8}$$

In Equation (8), P_{rated} is the rated output power of the wind turbine. v_{ci}, v_{co}, and v_{r} are the cut-in speed, cut-out speed, and rated speed of the wind turbine, respectively.

4. Expressway Microgrid Construction Mode and Capacity Configuration Optimization Design Model

4.1. Introduction of Carbon Trading Mechanism

4.1.1. Free Carbon Emission Allowance

In order to realize the low-carbon development of the transportation energy system, the impact of carbon emissions needs to be considered in the expressway microgrid design model. At present, the initial carbon emission allowances of each enterprise are allocated in a gratuitous manner. The initial free carbon emission allowances are allocated on the basis of unit capacity [25]. In the expressway microgrids, the main sources of carbon emissions are diesel generators in an islanded pattern and thermal generators' power from the distribution network in a grid-connected pattern. In this paper, it is assumed that the carbon emissions of each unit are proportional to the power output. When the actual carbon emissions of the system exceed the free allocation, the excess carbon emissions should be

purchased in a carbon trading market. The free carbon emission allowance allocated for the expressway microgrid can be expressed as Equation (9).

$$Q_{co_2} = (1 - I_n)\xi_g E_g + I_n \xi_{buy} \lambda_{buy} E_{buy} \tag{9}$$

In Equation (9), Q_{co_2} is the free carbon emission allowance. I_n is the decision variable for the grid-connected/islanded pattern (1 for grid-connected pattern, 0 for islanded pattern). ξ_g and ξ_{buy} are the carbon emission allowance of the unit electric power output of the diesel generators in an expressway microgrid and thermal generators in an external grid, respectively. E_g and E_{buy} are the electricity generated by diesel generators and external thermal generators, respectively. λ_{buy} is the ratio of electricity generated by thermal generators in the external grid.

4.1.2. Carbon Trading Model Considering Carbon Offset Mechanism

As a complementary mechanism to carbon emissions trading, the carbon offset mechanism originates from the clean development mechanism (CDM) and has spawned a project-based market with CER as a commodity [26]. Distributed power sources in microgrids can be declared as CER projects for offsetting system carbon emissions or listing for sale. The CER of an expressway microgrid can be expressed as Equation (10).

$$E_{CER} = \mu_{EFCM}(E_w + E_{PV}) \tag{10}$$

$$\mu_{EFCM} = 0.75\mu_{EFOM} + 0.25\mu_{EFBM} \tag{11}$$

In Equations (10) and (11), E_{CER} is the certified emission reduction. E_w and E_{PV} are the annual power generation of wind power and PV. μ_{EFCM}, μ_{EFOM}, and μ_{EFBM} are the emission factor of the operating margin, build margin and combined margin, respectively.

The actual carbon emissions of an expressway microgrid can be expressed as Equation (12).

$$E_{total} = (1 - I_n)\mu_g E_g + I_n \mu_{buy} \lambda_{buy} E_{buy} \tag{12}$$

In Equation (12), E_{total} is the actual carbon emissions before carbon offset mechanisms are taken into account. μ_g and μ_{buy} are the carbon emission factor for the diesel generators in an expressway microgrid and thermal generators in an external grid, respectively.

An excessive CER offset ratio will have a shock effect on the supply and demand relationship in the carbon trading market [27]. CERs' carbon offsets shall be constrained by Equation (13) and the benefit of trading CER residuals after offsetting carbon emissions can be expressed as follows.

$$E_{offset} = \min[E_{CER}, \beta_{offset} E_{total}] \tag{13}$$

$$C^{CER} = \lambda_{CER}(E_{CER} - E_{offset}) \tag{14}$$

In Equations (13) and (14), E_{offset} is the carbon offset allowances. β_{offset} is the maximum carbon offset ratio factor. C^{CER} is the expressway microgrid CER trading benefit. λ_{CER} is the CER trading price.

The net carbon emissions E_{co_2} of an expressway microgrid considering carbon offset mechanisms can be expressed as Equation (15).

$$E_{co_2} = E_{total} - E_{offset} \tag{15}$$

With the CER trading benefit, the carbon trading cost can be calculated as Equation (16).

$$C^{CT} = \varepsilon(E_{co_2} - Q_{co_2}) - C^{CER} \tag{16}$$

In Equation (16), C^{CT} is the carbon trading cost of the expressway microgrid. ε is the carbon trading price.

4.2. Objective Function

The objective of this paper is to minimize the annualized comprehensive cost of the expressway microgrid, which comprises the annualized investment cost, operational cost, and carbon trading cost. The objective function can be expressed as Equation (17).

$$\min\left[\lambda_{\mathrm{CRF}}\mathrm{C}^{\mathrm{INV}}+\frac{1}{Y}\sum_{y=1}^{Y}\left(C_{y}^{\mathrm{CT}}+365\sum_{s\in S}\omega_{s}C_{y,s}^{\mathrm{OP}}\right)\right]$$
$$\lambda_{\mathrm{CRF}}=\frac{i(1+i)^{Y}}{(1+i)^{Y}-1} \tag{17}$$

In Equation (17), C^{INV} and $C_{y,s}^{\mathrm{OP}}$ correspond to the total investment cost and daily operational cost in year y of the expressway microgrid, respectively. λ_{CRF} is the capital recovery factor. i is the discount rate. Y is the planned cycle of the expressway microgrid. S is the set of operating scenarios. ω_s is the probability of scenario s occurring.

4.2.1. Investment Cost

The total investment cost of an expressway microgrid includes the fixed investment cost, grid-connected pattern investment cost, islanded pattern investment cost, DC microgrid investment cost, and AC microgrid investment cost.

The fixed investment cost is the equipment cost that needs to be spent in any construction mode of the microgrid, including the cost of wind and PV power generation units, battery energy storage, and charging points. The grid-connected pattern investment cost is the additional cost of a microgrid in a grid-connected pattern, including the cost of the transmission lines, transformer, and converter. The islanded pattern investment cost is the cost of controllable generators required to ensure the reliable operation of the microgrid. The DC microgrid investment cost includes the cost of rectifiers for AC generator units, such as wind power generation and diesel, as well as inverters for AC loads in load centers. The AC microgrid investment cost includes the cost of SVCs, rectifiers for DC loads, and inverters for DC power generation equipment. Equations (20)–(23) are multiplied by their respective decision variables in Equation (18) in order to remove the cost of undecided modes.

$$C^{\mathrm{INV}}=C^{\mathrm{FIX}}+I_{\mathrm{n}}C^{\mathrm{GC}}+(1-I_{\mathrm{n}})C^{\mathrm{IS}}+I_{\mathrm{m}}C^{\mathrm{DC}}+(1-I_{\mathrm{m}})C^{\mathrm{AC}} \tag{18}$$

$$C^{\mathrm{FIX}}=\mathrm{c_w}P_{\mathrm{w}}^{\mathrm{N}}+\mathrm{c_{PV}}N_{\mathrm{PV}}P_{\mathrm{PV}}^{\mathrm{N}}+\mathrm{c}_{\mathrm{b}}^{\mathrm{P}}N_{\mathrm{b}}P_{\mathrm{b}}^{\mathrm{N}}+\mathrm{c}_{\mathrm{b}}^{\mathrm{E}}N_{\mathrm{b}}E_{\mathrm{b}}^{\mathrm{N}}+\mathrm{c}_{\mathrm{EV}}^{\mathrm{INV}}\mathrm{N_{EV}} \tag{19}$$

$$C^{\mathrm{GC}}=\mathrm{c_{line}L}^{\mathrm{GC}}+(\mathrm{c_{trans}}+I_{\mathrm{m}}\mathrm{c_{con}})P_{\mathrm{line}}^{\mathrm{N}} \tag{20}$$

$$C^{\mathrm{IS}}=\mathrm{c}_{\mathrm{g}}^{\mathrm{INV}}P_{\mathrm{g}}^{\mathrm{N}} \tag{21}$$

$$C^{\mathrm{DC}}=\mathrm{c_{rec}}\left[P_{\mathrm{w}}^{\mathrm{N}}+(1-I_{\mathrm{n}})P_{\mathrm{g}}^{\mathrm{N}}\right]+\mathrm{c_{inv}P_{L}^{max}} \tag{22}$$

$$C^{\mathrm{AC}}=\mathrm{c_{inv}}\left(P_{\mathrm{PV}}^{\mathrm{N}}+P_{\mathrm{b}}^{\mathrm{N}}\right)+\mathrm{c_{rec}P_{EV}^{N}N_{EV}}+\mathrm{c_{SVC}}Q_{\mathrm{SVC}}^{\mathrm{N}} \tag{23}$$

In Equations (18)–(23), C^{FIX}, C^{GC}, C^{IS}, C^{DC}, and C^{AC} correspond to the fixed investment cost, grid-connected pattern investment cost, islanded pattern investment cost, DC microgrid investment cost, and AC microgrid investment cost, respectively. I_{m} is the decision variable for the AC/DC type (1 for DC, 0 for AC). $\mathrm{c_w}$, $\mathrm{c_{PV}}$, and $\mathrm{c}_{\mathrm{EV}}^{\mathrm{INV}}$ are the unit capacity investment cost of wind power, the PV power unit, and the EV charging point, respectively. N_{PV} and N_{b} are the number of PV panel replacements in the planning cycle. $P_{\mathrm{w}}^{\mathrm{N}}$, $P_{\mathrm{PV}}^{\mathrm{N}}$, and $P_{\mathrm{g}}^{\mathrm{N}}$ are the installed capacity of wind power, PV power generation, and the diesel generator, respectively. $\mathrm{c}_{\mathrm{b}}^{\mathrm{P}}$ and $\mathrm{c}_{\mathrm{b}}^{\mathrm{E}}$ are the investment cost per unit of battery energy storage power and energy capacity, respectively. $P_{\mathrm{b}}^{\mathrm{N}}$ and $E_{\mathrm{b}}^{\mathrm{N}}$ are the power and energy capacity of battery energy storage, respectively. $\mathrm{c_{trans}}$, $\mathrm{c_{con}}$, $\mathrm{c_{inv}}$, $\mathrm{c_{rec}}$, and $\mathrm{c_{line}}$ are

the investment cost per unit capacity of the transformers, converters, inverters, rectifiers, and per unit length of the transmission line, respectively. L^{GC} and P_{line}^{N} are the length and capacity of transmission line. c_g^{INV} is the unit capacity investment cost of the diesel generator. P_L^{max}, P_{EV}^{N}, and N_{EV} are the maximum AC load and the power and number of single charging points, respectively. c_{SVC} and Q_{SVC}^{N} are the investment cost per unit capacity and installed capacity of SVC.

4.2.2. Operational Cost

The operational cost includes the fuel cost in an islanded pattern and the power trading cost with the distribution network in a grid-connected pattern. For the purposes of simplification and enhanced representation, the subscript y is dropped from all the variables as follows.

$$C_s^{OP} = (1 - I_n)C_s^{FUEL} + I_n C_s^{LINE} \tag{24}$$

$$C_s^{FUEL} = \sum_{t \in T} I_{s,t}^{g} \left(a_g P_{s,t}^{g} + b_g P_g^{N} \right) \tag{25}$$

$$C_s^{LINE} = \sum_{t \in T} \left(c_t^{buy} P_{s,t}^{buy} - c_t^{sell} P_{s,t}^{sell} \right) \Delta t \tag{26}$$

In Equations (24)–(26), C_s^{FUEL} and C_s^{LINE} are the fuel cost and power trading cost, respectively. Note that the cost of power trading is negative when the revenue of power sales is greater than the cost of power purchase. $I_{s,t}^{g}$ is the on–off variable of the diesel generator. a_g and b_g are the cost factors for the diesel generator. $P_{s,t}^{g}$ is the actual active power output of the diesel generator. c_t^{buy} and c_t^{sell} are the purchase and sale price of electricity at time t, respectively. $P_{s,t}^{buy}$ and $P_{s,t}^{sell}$ are the actual purchase and sale active power between the expressway microgrid and distribution network, respectively. T is the set of time periods.

4.3. Constraints

4.3.1. Power Balance Constraints

The active power generated by the components within the microgrid and purchased from the distribution network must meet the active load demand. In particular, AC microgrids also need to satisfy the balance between reactive power output and reactive load demand.

$$P_{s,t}^{w'} + P_{s,t}^{PV'} + P_{s,t}^{dis'} + (1 - I_n)P_{s,t}^{g'} + I_n P_{s,t}^{buy'} = P_{s,t}^{L'} + P_{s,t}^{EV'} + P_{s,t}^{ch'} + I_n P_{s,t}^{sell'} \tag{27}$$

$$(1 - I_m)\left[Q_{s,t}^{w} + Q_{s,t}^{PV} + Q_{s,t}^{dis} + (1 - I_n)Q_{s,t}^{g} + I_n Q_{s,t}^{buy} + Q_{s,t}^{SVC} - Q_{s,t}^{L} \right] = 0 \tag{28}$$

In Equation (27), $P_{s,t}^{*'}$ refers to the net active power considering the converter losses of the corresponding component in the AC/DC expressway microgrid. $Q_{s,t}^{w}$, $Q_{s,t}^{g}$, and $Q_{s,t}^{buy}$ are the reactive power of wind power generation, diesel, and the transmission line, respectively. $Q_{s,t}^{PV}$ and $Q_{s,t}^{dis}$ are the reactive power of the inverters between these DC components and the AC bus. $Q_{s,t}^{SVC}$ is the reactive power of SVC. $Q_{s,t}^{L}$ is the reactive load demand.

4.3.2. Renewable Energy Installed Capacity Constraints

Wind and PV power generation installations are constrained by the amount of available l and area. The exploitable area near the expressway load center is limited, so the installed capacity of an expressway microgrid cannot exceed the maximum exploitable limit.

$$0 \le P_w^{N} \le P_w^{Nmax} \tag{29}$$

$$0 \le P_{PV}^{N} \le P_{PV}^{Nmax} \tag{30}$$

In Equations (29) and (30), $P_{\mathrm{w}}^{\mathrm{Nmax}}$ and $P_{\mathrm{PV}}^{\mathrm{Nmax}}$ are the maximum exploitable wind and PV power generation installed capacity in the load center, respectively.

4.3.3. Renewable Energy Output Constraints

Wind and PV power output is limited by the maximum available output, which can be calculated using the methodology in Section 3. Component aging will lead to a significant decrease in the PV module efficiency. In order to indicate this feature, Equation (31) uses the PV module efficiency decay coefficient to limit the actual PV output.

$$0 \le P_{s,t}^{\mathrm{w}} \le \alpha_{s,t} P_{\mathrm{w}}^{\mathrm{N}} \tag{31}$$

$$0 \le P_{s,t}^{\mathrm{PV}} \le \beta_{s,t}\left(1 - \eta_{\mathrm{de}}^{\mathrm{PV}} Y_{\mathrm{PV}}\right) P_{\mathrm{PV}}^{\mathrm{N}} \tag{32}$$

$$0 \le {P_{s,t}^{\mathrm{w}}}^2 + (1 - I_m){Q_{s,t}^{\mathrm{w}}}^2 \le {P_{\mathrm{w}}^{\mathrm{N}}}^2 \tag{33}$$

$$0 \le {P_{s,t}^{\mathrm{PV}}}^2 + (1 - I_m){Q_{s,t}^{\mathrm{PV}}}^2 \le {P_{\mathrm{PV}}^{\mathrm{N}}}^2 \tag{34}$$

$$P_{s,t}^{\mathrm{w}'} = [\eta_{\mathrm{ACDC}} I_{\mathrm{m}} + (1 - I_{\mathrm{m}})] P_{s,t}^{\mathrm{w}} \tag{35}$$

$$P_{s,t}^{\mathrm{PV}'} = [I_{\mathrm{m}} + (1 - I_{\mathrm{m}})\eta_{\mathrm{DCAC}}] P_{s,t}^{\mathrm{PV}} \tag{36}$$

In Equations (31)–(36), $\alpha_{s,t}$ and $\beta_{s,t}$ are the maximum available output per unit value of wind and PV power, respectively. $P_{s,t}^{\mathrm{w}}$ and $P_{s,t}^{\mathrm{PV}}$ are the actual active output of wind power and PV power generation in scenario s at time t, respectively. $\eta_{\mathrm{de}}^{\mathrm{PV}}$ is the PV power generation efficiency decay coefficient. Y_{PV} is the usage time of the PV module. η_{ACDC} and η_{DCAC} are the AC/DC and DC/AC conversion efficiency, respectively.

4.3.4. Diesel Generator Output Constraints

The active and reactive power outputs of diesel generator are limited by the installed capacity.

$$P_{\mathrm{g}}^{\mathrm{min}} \le P_{s,t}^{\mathrm{g}} \le P_{\mathrm{g}}^{\mathrm{N}} \tag{37}$$

$$0 \le {P_{s,t}^{\mathrm{g}}}^2 + (1 - I_m){Q_{s,t}^{\mathrm{g}}}^2 \le {P_{\mathrm{g}}^{\mathrm{N}}}^2 \tag{38}$$

$$P_{s,t}^{\mathrm{g}'} = [\eta_{\mathrm{ACDC}} I_{\mathrm{m}} + (1 - I_{\mathrm{m}})] P_{s,t}^{\mathrm{g}} \tag{39}$$

In Equation (37), $P_{\mathrm{g}}^{\mathrm{min}}$ is the minimum active output of the diesel generator.

4.3.5. Battery Energy Storage Constraints

One lithium battery was introduced to the optimization model. Equation (40) limits the charging and discharging power of the battery energy storage to be less than the power capacity. Equation (42) guarantees that the charging and discharging power cannot be positive at the same time. The change of stored electricity can be calculated as indicated in Equation (44). Equation (45) limits the lower and upper limits of the state of charge, which takes into account the decrease in energy capacity of the battery energy storage. Equation (46) ensures that the beginning and end states are consistent.

$$0 \le P_{s,t}^{\mathrm{ch}}, P_{s,t}^{\mathrm{dis}} \le P_{\mathrm{b}}^{\mathrm{N}} \tag{40}$$

$$0 \le {P_{s,t}^{\mathrm{dis}}}^2 + (1 - I_m){Q_{s,t}^{\mathrm{dis}}}^2 \le {P_{\mathrm{b}}^{\mathrm{N}}}^2 \tag{41}$$

$$0 \le P_{s,t}^{\mathrm{ch}} \perp P_{s,t}^{\mathrm{dis}},\ Q_{s,t}^{\mathrm{dis}} \ge 0 \tag{42}$$

$$\begin{cases} P_{s,t}^{\mathrm{ch}'} = [I_{\mathrm{m}} + (1 - I_{\mathrm{m}})/\eta_{\mathrm{ACDC}}]P_{s,t}^{\mathrm{ch}} \\ P_{s,t}^{\mathrm{dis}'} = [I_{\mathrm{m}} + (1 - I_{\mathrm{m}})\eta_{\mathrm{DCAC}}]P_{s,t}^{\mathrm{dis}} \end{cases} \tag{43}$$

$$E_{s,t+1} = E_{s,t} + \left(\eta_{\mathrm{ch}} P_{s,t}^{\mathrm{ch}} - P_{s,t}^{\mathrm{dis}}/\eta_{\mathrm{dis}}\right)\Delta t \tag{44}$$

$$E_{\mathrm{b}}^{\min} \le E_{s,t} \le \left(1 - \eta_{\mathrm{de}}^{\mathrm{b}} Y_{\mathrm{b}}\right) E_{\mathrm{b}}^{\max} \tag{45}$$

$$E_{s,0} = E_{s,T} \tag{46}$$

In Equations (40)–(45), $P_{s,t}^{\mathrm{ch}}$ and $P_{s,t}^{\mathrm{dis}}$ are the actual charging and discharging active power of the battery energy storage. $E_{s,t}$ is the electricity stored by the battery energy storage. η_{ch} and η_{dis} are the charging and discharging efficiency, respectively. $E_{\mathrm{b}}^{\min}$ and $E_{\mathrm{b}}^{\max}$ are the minimum and maximum electricity stored by the battery energy storage, respectively. $\eta_{\mathrm{de}}^{\mathrm{b}}$ is the battery capacity decay coefficient. Y_{b} is the usage time of battery energy storage.

4.3.6. Transmission Line Constraints

The power purchased and sold between the microgrid and distribution network are limited by the capacity and power factor of transmission line.

$$0 \le P_{s,t}^{\mathrm{buy}}, P_{s,t}^{\mathrm{sell}} \le P_{\mathrm{line}}^{\mathrm{N}} \tag{47}$$

$$0 \le {P_{s,t}^{\mathrm{buy}}}^2 + (1 - I_m){Q_{s,t}^{\mathrm{buy}}}^2 \le {P_{\mathrm{line}}^{\mathrm{N}}}^2 \tag{48}$$

$$\cos\varphi_{\mathrm{line}} \le P_{s,t}^{\mathrm{buy}} \Big/ \sqrt{{P_{s,t}^{\mathrm{buy}}}^2 + (1 - I_m){Q_{s,t}^{\mathrm{buy}}}^2} \tag{49}$$

$$0 \le P_{s,t}^{\mathrm{sell}} \perp P_{s,t}^{\mathrm{buy}},\ Q_{s,t}^{\mathrm{buy}} \ge 0 \tag{50}$$

$$\begin{cases} P_{s,t}^{\mathrm{buy}'} = [\eta_{\mathrm{ACDC}} I_{\mathrm{m}} + (1 - I_{\mathrm{m}})]\eta_{\mathrm{line}} P_{s,t}^{\mathrm{buy}} \\ P_{s,t}^{\mathrm{sell}'} = [I_{\mathrm{m}}/\eta_{\mathrm{DCAC}} + (1 - I_{\mathrm{m}})]P_{s,t}^{\mathrm{sell}}/\eta_{\mathrm{line}} \end{cases} \tag{51}$$

In Equations (47)–(51), η_{line} is the transmission efficiency of the transmission line. $\cos\varphi_{\mathrm{line}}$ is the power factor limit of the transmission line.

4.3.7. AC/DC Load Constraint

The following load constraints consider the power loss in electronic converters.

$$\begin{cases} P_{s,t}^{\mathrm{L}'} = [I_{\mathrm{m}}/\eta_{\mathrm{DCAC}} + (1 - I_{\mathrm{m}})]P_{s,t}^{\mathrm{L}} \\ P_{s,t}^{\mathrm{EV}'} = [I_{\mathrm{m}} + (1 - I_{\mathrm{m}})/\eta_{\mathrm{ACDC}}]P_{s,t}^{\mathrm{EV}} \end{cases} \tag{52}$$

In Equation (52), $P_{s,t}^{\mathrm{L}}$ and $P_{s,t}^{\mathrm{EV}}$ are the actual active power of the AC and DC loads, respectively.

4.3.8. SVC Constraint

The output reactive power of the SVC must be less than the installed capacity.

$$0 \le (1 - I_m)Q_{s,t}^{\mathrm{SVC}} \le Q_{\mathrm{SVC}}^{\mathrm{N}} \tag{53}$$

In Equation (53), $Q_{s,t}^{\mathrm{SVC}}$ is the reactive power of SVC in the AC microgrid.

5. Case Study

5.1. Basic Data

This paper uses an expressway in the east of China as an example. According to the local renewable energy output and load data, the typical scenarios of renewable energy output and load can be selected as shown in Figure 2. The investment cost factors, power efficiency, and related parameters of each component in the expressway microgrid are shown in Table 1 [28–32]. The grid-connected distance of the expressway microgrid is 20 km. The maximum AC and DC loads are 200 kW and 500 kW. The maximum installed capacities of wind and PV power generation that can be deployed are 500 kW and 1500 kW, respectively. The planning cycle is 20 years, and the discount rate is taken as 8%. The expressway microgrid design model presented in this paper is a mixed integer nonlinear programming problem, which can be solved in GUROBI through the MATLAB platform.

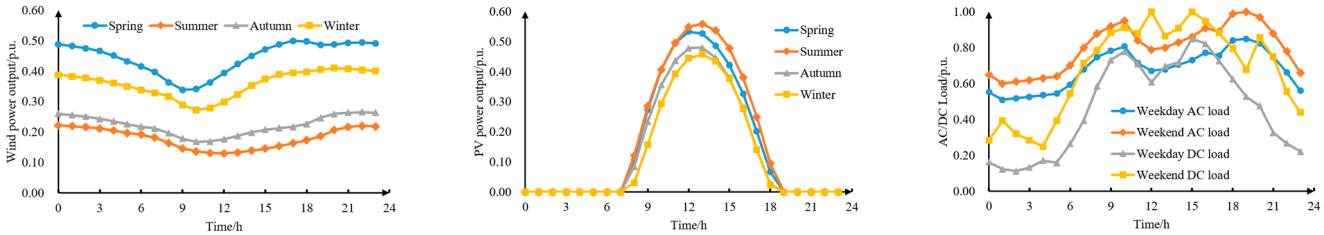

(**a**) (**b**) (**c**)

Figure 2. (**a**) Wind power output of typical weather throughout the year; (**b**) PV power output of typical weather throughout the year; (**c**) AC/DC load demand of expressway microgrid.

Table 1. The investment cost factors and related parameters.

Parameter	Value	Parameter	Value	Parameter	Value
c_w (USD/kW)	825	c_{line} (USD/kW)	120	a_g (USD/kW)	0.1
c_{PV} (USD/kW)	525	c_{con} (USD/kW)	140	b_g (USD/kW)	0.03
c_g^{INV} (USD/kW)	200	c_{inv} (USD/kW)	140	η_{ACDC} & η_{DCAC}	0.96
c_b^P (USD/kW)	150	c_{rec} (USD/kW)	140	η_{ch} & η_{dis} & η_{line}	0.95
c_b^E (USD/kWh)	180	c_{trans} (USD/kW)	788	c_{SVC} (USD/kvar)	30
ξ_g (kg/kWh)	0.50	μ_g (kg/kWh)	0.65	ε (USD/t)	40
ξ_{buy} (kg/kWh)	0.78	μ_{buy} (kg/kWh)	0.92	λ_{CER} (USD/t)	20

In order to verify the validity and practicality of the proposed model in different scenarios, the following scenarios are constructed in this paper:

(a) Scenario a is the base scenario represented by the data above, which is applicable to a normal expressway microgrid that contains AC and DC loads.

(b) Scenario b reduces the grid-connected distance to 5 km on the basis of scenario a, which is applicable to expressway load centers close to the point of common coupling.

(c) Scenario c adds the maximum deployable capacity of PV power generation to 3000 kW, which is the deployable capacity in the available area of the expressway side slopes around the load center. This scenario is applicable to load centers on east–west expressways, whose side slopes are able to make full use of PV resources, while north–south expressways are not.

(d) Scenario d eliminates the DC loads on the basis of scenario a. This scenario is applicable to expressway microgrids that contain only AC loads, such as tunnels and service areas without charging points.

5.2. Optimization Results and Analysis of Different Scenarios

The purpose of this section is to demonstrate the validity and applicability of the design model proposed in this paper under different possible expressway microgrid scenarios.

5.2.1. Scenario a

The construction mode in this scenario is mode 3, and the comprehensive cost is USD 306,856. The results of the capacity configuration and annualized comprehensive cost of the expressway microgrid under different construction modes are shown in Table 2 and Figure 3.

Table 2. The capacity configuration of scenario a under different modes.

Capacity Configuration	Mode 1	Mode 2	Mode 3	Mode 4
Wind power generation (kW)	500	500	500	500
PV power generation (kW)	1500	1500	1500	1500
Battery energy storage power capacity (kW)	251	241	225	158
Battery energy storage energy capacity (kWh)	1105	1284	1155	750
Diesel generator (kW)	0	0	344	394
Transmission line (kW)	366	360	0	0
SVC capacity (kvar)	0	20	0	28
Annualized comprehensive cost (USD)	316,668	343,093	306,856	323,184

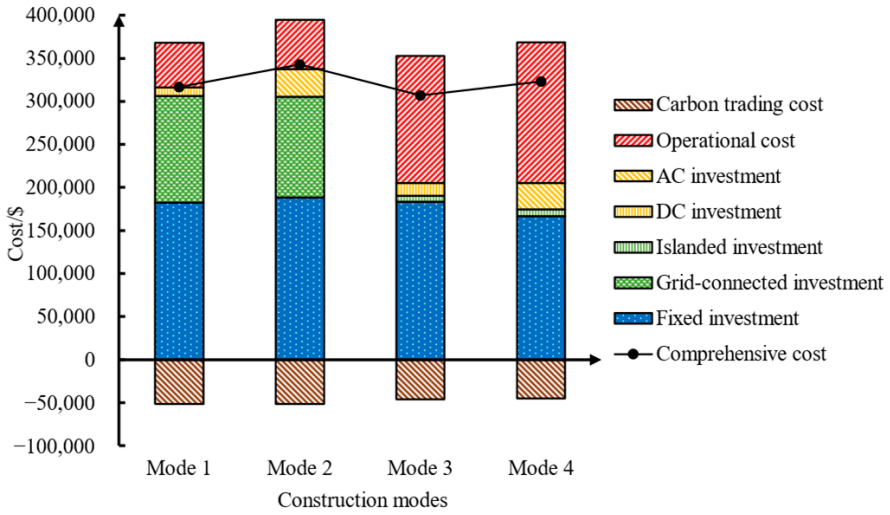

Figure 3. The economic index of scenario a under different modes.

In this scenario, the renewable energy resources are very limited. Large capacity transmission lines or diesel generators are required to meet the load demand. Because of the higher unit price, the grid-connected investment in modes 1 and 2 is much higher than the islanded investment in modes 3 and 4. Even though the grid-connected pattern has lower operational costs for purchasing power from the grid, the low operational costs can hardly compensate for the high grid-connected investment costs due to the large investment of transmission lines, which leads to a higher comprehensive cost than the islanded pattern. Moreover, because of the higher DC load demand in scenario a, the investment and operational costs of a DC microgrid are lower than AC. As shown in Figure 3, it is more economical to build an islanded DC expressway microgrid in scenario a.

5.2.2. Scenario b

The construction mode in this scenario is mode 1, and the comprehensive cost is USD 246,838. The results of the capacity configuration and annualized comprehensive cost of the expressway microgrid under different construction modes are shown in Table 3 and Figure 4.

Table 3. The capacity configuration of scenario b under different modes.

Capacity Configuration	Mode 1	Mode 2	Mode 3	Mode 4
Wind power generation (kW)	500	500	500	500
PV power generation (kW)	1500	1500	1500	1500
Battery energy storage power capacity (kW)	176	161	225	158
Battery energy storage energy capacity (kWh)	689	560	1155	750
Diesel generator (kW)	0	0	344	394
Transmission line (kW)	396	404	0	0
SVC capacity (kvar)	0	59	0	28
Annualized comprehensive cost (USD)	246,838	265,343	306,856	323,184

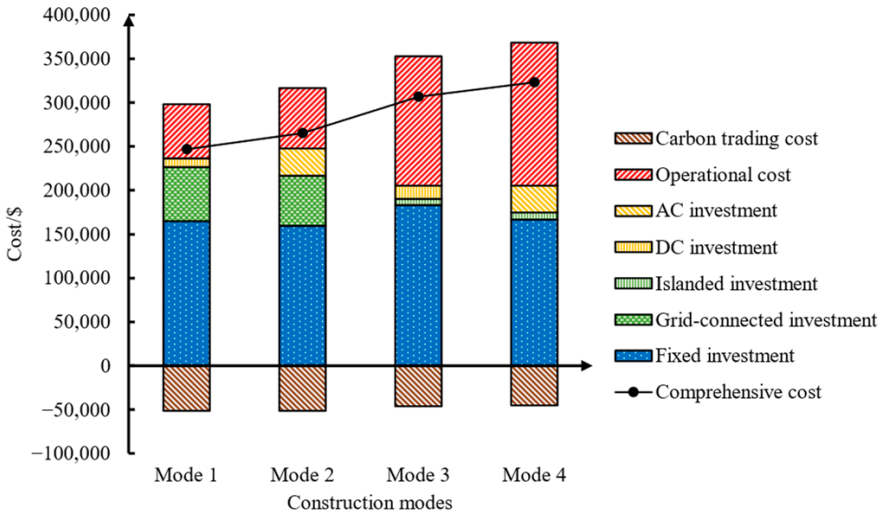

Figure 4. The economic index of scenario b under different modes.

Compared with scenario a, scenario b is close to the point of common coupling and has lower transmission line costs per unit capacity. As a result, mode 1 enables the lowest comprehensive investment cost while increasing the transmission line capacity to reduce the capacity requirements of the battery energy storage.

5.2.3. Scenario c

The construction mode in this scenario is mode 1, and the comprehensive cost is USD 294,699. The results of the capacity configuration and annualized comprehensive cost of the expressway microgrid under different construction modes are shown in Table 4 and Figure 5.

Table 4. The capacity configuration of scenario c under different modes.

Capacity Configuration	Mode 1	Mode 2	Mode 3	Mode 4
Wind power generation (kW)	500	500	500	500
PV power generation (kW)	2254	2120	1860	1847
Battery energy storage power capacity (kW)	273	216	311	280
Battery energy storage energy capacity (kWh)	1211	1005	1914	1643
Diesel generator (kW)	0	0	288	308
Transmission line (kW)	346	359	0	0
SVC capacity (kvar)	0	16	0	5
Annualized comprehensive cost (USD)	294,699	325,899	294,942	318,934

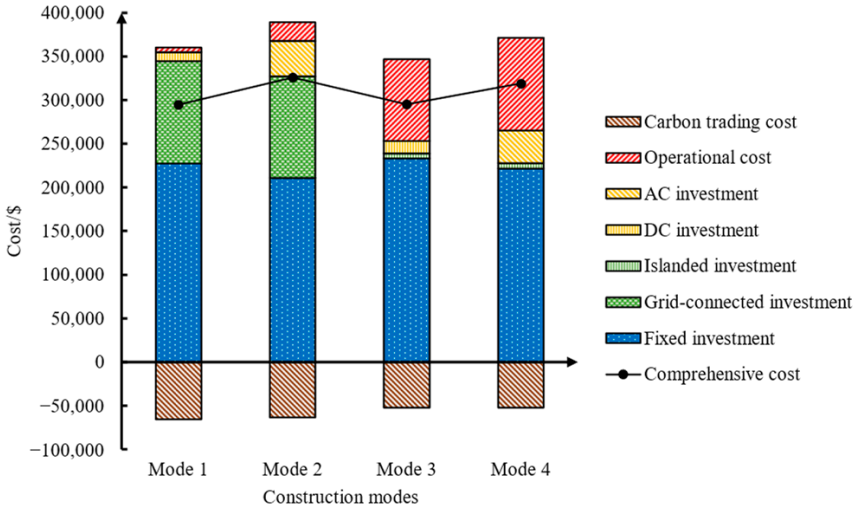

Figure 5. The economic index of scenario c under different modes.

Compared with scenario a, the grid-connected investment in scenario c is still higher than the islanded investment cost, but due to the larger exploitable resources, the grid-connected pattern (mode 1) can sell the excess PV power to the distribution network, which saves operational costs and even achieves profit.

5.2.4. Scenario d

The construction mode in scenario d is mode 2, whose comprehensive cost is USD 55,601. The results of the capacity configuration and annualized comprehensive cost of the expressway microgrid under different construction modes are shown in Table 5 and Figure 6.

Table 5. The capacity configuration of scenario d under different modes.

Capacity Configuration	Mode 1	Mode 2	Mode 3	Mode 4
Wind power generation (kW)	500	500	500	500
PV power generation (kW)	344	238	245	190
Battery energy storage power capacity (kW)	46	31	35	10
Battery energy storage energy capacity (kWh)	134	73	93	31
Diesel generator (kW)	0	0	87	97
Transmission line (kW)	80	82	0	0
SVC capacity (kvar)	0	92	0	88
Annualized comprehensive cost (USD)	66,251	55,601	71,193	57,098

There is no DC load and few PV installations in scenario d, which leads to the construction of a DC microgrid without any advantage compared to an AC microgrid under the same grid connection pattern, even though the AC microgrids need to be configured with SVC, as shown in Figure 6. Benefiting from a lower load demand, mode 2 becomes the optimal mode for the key reason of lower operational costs.

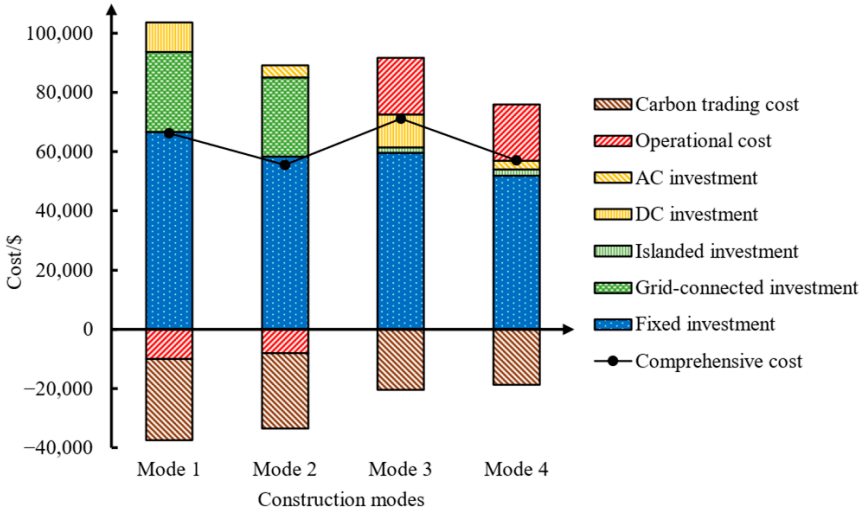

Figure 6. The economic index of scenario d under different modes.

5.3. Comparison between Different Carbon Trading Models

To indicate the necessity of considering carbon trading for expressway microgrid construction modes and capacity configuration optimization, this section presents a comparative analysis of the following three design models based on scenario c: (a) without considering a carbon offset mechanism and carbon trading costs; (b) only considering carbon trading costs; (c) considering both carbon trading costs and a carbon offset mechanism. The planning results of the different models are shown in Table 6.

Table 6. The planning results of different carbon trading models.

Planning Result	Model a	Model b	Model c
Construction mode	Mode 3	Mode 3	Mode 1
Wind power generation (kW)	500	500	500
PV power generation (kW)	1805	1805	2254
Battery energy storage power capacity (kW)	288	288	273
Battery energy storage energy capacity (kWh)	1744	1744	1211
Diesel generator (kW)	300	300	0
Transmission line (kW)	0	0	346

As the main power source in an expressway microgrid, renewable energy generation substantially reduces the level of microgrid carbon emissions. If the carbon offset mechanism is not taken into account, the low cost of carbon emission trading is not enough to incentivize the microgrid to increase the installed capacity of renewable energy and the battery energy storage to reduce the carbon emissions of the system. When the carbon offset mechanism is considered in the design model, the construction mode converts from mode 3 to mode 1 as the grid-connected pattern is able to consume a large amount of renewable energy generation, which provides a significant benefit to the microgrid. Meanwhile, the renewable energy and battery energy storage capacity configurations have also been increased. It can be seen that considering a carbon offset mechanism will have a significant impact on the planning results.

5.4. Sensitivity Analysis of the CER Trading Price

This section explores the sensitivity analysis of different CER trading prices according to the proposed scenario c. The CER trading price changes from 10 to 30 USD/t, and the expressway microgrid planning results are represented in Table 7.

As shown in Table 7, when the CER trading price is lower than 20 USD/t, the lower CER trading benefit cannot motivate the model to select a grid-connected pattern; therefore, mode 3 is the optimal construction mode. When the trading price is higher than 20 USD/t, the grid-connected pattern (mode 1) is able to expand the installed PV capacity and transmission line capacity to increase the CER trading benefit by selling the excess PV power generation; however, when the CER trading price is higher than 25 USD/t, an additional configuration of the battery energy storage is needed to consume the excess PV power, which leads to the CER trading benefit being insufficient to compensate for the additional battery investment cost. Therefore, the optimal configuration result will no longer change with the increase in the CER trading price. This section indicates that the CER trading price will affect the expressway microgrid planning results. It is necessary to consider the impact of the CER trading price uncertainty on expressway microgrid planning in future studies.

Table 7. The planning results under different CER trading price.

CER Trading Price (USD/t)	10	15	20	25	30
Construction mode	Mode 3	Mode 3	Mode 1	Mode 1	Mode 1
Wind power generation (kW)	500	500	500	500	500
PV power generation (kW)	1805	1807	2254	2325	2325
Battery energy storage power capacity (kW)	288	288	273	303	303
Battery energy storage energy capacity (kWh)	1744	1743	1211	1211	1211
Diesel generator (kW)	300	300	0	0	0
Transmission line (kW)	0	0	346	346	346
Annualized comprehensive cost (USD)	321,414	308,226	294,699	277,997	261,217

6. Conclusions

This paper presents a design model for expressway microgrids. Considering different ratios of renewable energy exploitable capacity and load structure, the model is designed to decide the construction mode and component capacity size of expressway microgrids, such as renewable energy generation, battery energy storage, converters, etc. The problem is formulated as an MINLP, which minimizes the annualized comprehensive cost under system and component constraints. The annualized comprehensive cost includes the investment cost, operational cost, and carbon trading cost. Of significance, the model considers carbon trading and a carbon offset mechanism, as well as the relationship between the actual power and net power under different construction modes.

This paper analyzes several case studies and application scenarios to prove the validity and practicality of the proposed model. This paper indicates that the expressway microgrid construction mode is impacted by the renewable energy exploitable limit, grid connection distance, and load structure. When the type of expressway microgrid is considered as a decision variable, the annualized comprehensive cost is significantly reduced. More importantly, the case studies show that considering carbon trading and offset mechanisms will affect the expressway microgrid planning results. It is necessary to consider the uncertainty of the CER trading price in future studies.

Author Contributions: Conceptualization, L.Y. and S.L.; methodology, L.Y. and C.B.; software, H.F.; validation, C.B., H.F. and S.L.; formal analysis, L.Y. and C.B.; investigation, Y.F.; resources, L.Y.; data curation, Y.F.; writing—original draft preparation, L.Y.; writing—review and editing, S.L.; visualization, C.B.; supervision, H.F.; project administration, L.Y.; funding acquisition, H.F. All authors have read and agreed to the published version of the manuscript.

Funding: This study was funded by the Major Science and Technology Projects of Transportation and Energy Integration in China Energy Construction Co., Ltd. (CEEC2021-KJZX-08-1).

Data Availability Statement: The numerical data used to support the findings of this study are included within the article.

Conflicts of Interest: The authors declare no conflict of interest.

References

1. Song, M.; Zheng, W.; Wang, Z. Environmental efficiency and energy consumption of highway transportation systems in China. *Int. J. Prod. Econ.* **2016**, *181*, 441–449. [CrossRef]
2. Ye, Y.; Shi, R.; Gao, Y.; Ma, X.; Wang, D. Two-Stage Optimal Scheduling of Highway Self-Consistent Energy System in Western China. *Energies* **2023**, *16*, 2435. [CrossRef]
3. Jia, L.; Ma, J.; Cheng, P.; Liu, Y. A Perspective on Solar Energy-powered Road and Rail Transportation in China. *CSEE J. Power Energy Syst.* **2020**, *6*, 760–771.
4. Ding, Z.; Zhang, Y.; Tan, W.; Pan, X.; Tang, H. Pricing Based Charging Navigation Scheme for Highway Transportation to Enhance Renewable Generation Integration. *IEEE Trans. Ind. Appl.* **2023**, *59*, 108–117. [CrossRef]
5. Hafez, O.; Bhattacharya, K. Optimal design of electric vehicle charging stations considering various energy resources. *Renew. Energy* **2017**, *107*, 576–589. [CrossRef]
6. Shoji, T.; Noda, T. A study of harmonics in a dedicated cable supply system to feed EV fast chargers. *Electr. Power Syst. Res.* **2023**, *221*, 109421. [CrossRef]
7. Hu, Z.C.; Song, Y.H.; Xu, Z.W.; Luo, Z.W.; Zhan, K.Q.; Jia, L. Impacts and Utilization of Electric Vehicles Integration into Power Systems. *Proc. Chin. Soc. Electr. Eng.* **2012**, *32*, 1–10.
8. Pires, V.F.; Pires, A.; Cordeiro, A. DC Microgrids: Benefits, Architectures, Perspectives and Challenges. *Energies* **2023**, *16*, 1217. [CrossRef]
9. Li, Z.; Zhao, B.; Chen, Z.; Ni, C.; Yan, J.; Yan, X.; Bian, X.; Liu, N. Low-carbon operation method of microgrid considering carbon emission quota trading. *Energy Rep.* **2023**, *9*, 379–387. [CrossRef]
10. Bae, S.; Kwasinski, A. Spatial and Temporal Model of Electric Vehicle Charging Demand. *IEEE Trans. Smart Grid* **2012**, *3*, 394–403. [CrossRef]
11. Liu, H.; Li, R.; Ge, S.Y.; Wang, L.; Han, J. Multi-objective Planning of Electric Vehicle Charging Stations on Expressway Based on Dynamic Traffic Flow Simulation. *Autom. Electr. Power Syst.* **2015**, *39*, 56–62+79.
12. Ge, S.Y.; Zhu, L.W.; Liu, H.; Li, T.; Liu, C. Optimal Deployment of Electric Vehicle Charging Stations on the Highway Based on Dynamic Traffic Simulation. *Trans. China Electrotech. Soc.* **2018**, *33*, 2991–3001.
13. Rousis, A.O.; Konstantelos, I.; Strbac, G. A Planning Model for a Hybrid AC-DC Microgrid Using a Novel GA/AC OPF Algorithm. *IEEE Trans. Power Syst.* **2020**, *35*, 227–237. [CrossRef]
14. Lotfi, H.; Khodaei, A. AC Versus DC Microgrid Planning. *IEEE Trans. Smart Grid* **2017**, *8*, 296–304. [CrossRef]
15. Hamad, A.A.; Nassar, M.E.; El-Saadany, E.F.; Salama, M.M.A. Optimal Configuration of Isolated Hybrid AC/DC Microgrids. *IEEE Trans. Smart Grid* **2019**, *10*, 2789–2798. [CrossRef]
16. Cleenwerck, R.; Azaioud, H.; Vafaeipour, M.; Coosemans, T.; Desmet, J. Impact Assessment of Electric Vehicle Charging in an AC and DC Microgrid: A Comparative Study. *Energies* **2023**, *16*, 3205. [CrossRef]
17. John, B.; Ghosh, A.; Goyal, M.; Zare, F. A DC Power Exchange Highway Based Power Flow Management for Interconnected Microgrid Clusters. *IEEE Syst. J.* **2019**, *13*, 3347–3357. [CrossRef]
18. Ning, F.; Ji, L.; Ma, J.; Jia, L.; Yu, Z. Research and analysis of a flexible integrated development model of railway system and photovoltaic in China. *Renew. Energy* **2021**, *175*, 853–867. [CrossRef]
19. D'Arco, S.; Piegari, L.; Tricoli, P. Comparative Analysis of Topologies to Integrate Photovoltaic Sources in the Feeder Stations of AC Railways. *IEEE Trans. Transp. Electrif.* **2018**, *4*, 951–960. [CrossRef]
20. Tabar, V.S.; Jirdehi, M.A.; Hemmati, R. Sustainable planning of hybrid microgrid towards minimizing environmental pollution, operational cost and frequency fluctuations. *J. Clean. Prod.* **2018**, *203*, 1187–1200. [CrossRef]
21. Wang, R.; Wen, X.; Wang, X.; Fu, Y.; Zhang, Y. Low carbon optimal operation of integrated energy system based on carbon capture technology, LCA carbon emissions and ladder-type carbon trading. *Appl. Energy* **2022**, *311*, 118664. [CrossRef]
22. Feng, F.; Du, X.; Si, Q.; Cai, H. Hybrid Game Optimization of Microgrid Cluster (MC) Based on Service Provider (SP) and Tiered Carbon Price. *Energies* **2022**, *15*, 5291. [CrossRef]
23. Atwa, Y.M.; El-Saadany, E.F.; Salama, M.M.A.; Seethapathy, R.; Assam, M.; Conti, S. Adequacy Evaluation of Distribution System Including Wind/Solar DG during Different Modes of Operation. *IEEE Trans. Power Syst.* **2011**, *26*, 1945–1952. [CrossRef]
24. Zhao, B.; Zhang, X.; Chen, J.; Wang, C.; Guo, L. Operation Optimization of Standalone Microgrids Considering Lifetime Characteristics of Battery Energy Storage System. *IEEE Trans. Sustain. Energy* **2013**, *4*, 934–943. [CrossRef]
25. Wang, L.; Dong, H.; Lin, J.; Zeng, M. Multi-objective optimal scheduling model with IGDT method of integrated energy system considering ladder-type carbon trading mechanism. *Int. J. Electr. Power Energy Syst.* **2022**, *143*, 108386. [CrossRef]
26. Li, L.X.; Ye, F.; Li, Y.N.; Chang, C.-T. How will the Chinese Certified Emission Reduction scheme save cost for the national carbon trading system? *J. Environ. Manag.* **2019**, *244*, 99–109. [CrossRef]
27. Yu, J.; Mallory, M.L. Carbon price interaction between allocated permits and generated offsets. *Oper. Res.* **2020**, *20*, 671–700. [CrossRef]
28. Naderipour, A.; Saboori, H.; Mehrjerdi, H.; Jadid, S.; Abdul-Malek, Z. Sustainable and reliable hybrid AC/DC microgrid planning considering technology choice of equipment. *Sustain. Energy Grids Netw.* **2020**, *23*, 100386. [CrossRef]

29. Liang, S.H.; Lou, S.H.; Wu, Y.W.; Peng, Y. Generation Expansion Planning for Solvent-Storaged Carbon Capture Power Plants Considering the Internalization of the Carbon Emission Effects. *IEEE Trans. Power Syst.* **2023**, 1–15. [CrossRef]
30. Zhang, H.; Moura, S.J.; Hu, Z.; Song, Y. PEV Fast-Charging Station Siting and Sizing on Coupled Transportation and Power Networks. *IEEE Trans. Smart Grid* **2018**, *9*, 2595–2605. [CrossRef]
31. Xiao, B.; Liu, J.K.; Zhang, B.; Wu, F.Z. Optimal configuration of grid-connected microgrid with hydrogen energy storage considering ladder-type carbon trading and demand response. *Electr. Power Autom. Equip.* **2023**, *43*, 121–129.
32. Che, Q.H.; Wu, Y.W.; Zhu, Z.G.; Lou, S.H. Carbon Trading Based Optimal Scheduling of Hybrid Energy Storage System in Power Systems with Large-scale Photovoltaic Power Generation. *Autom. Electr. Power Syst.* **2019**, *43*, 76–82+154.